Supporting Information

Supporting Information Part I:

Table.1 the descriptions of N_2 adsorption–desorption isotherms for porous UNs

Values / Porous materials		Average pore defect size (nm)	BET surface area (m^2/g)	Pore volume (cm^3/g)
$NaYF_4$	Y:F=1:4	2.051907	3.900705	0.226699
	Y:F=1:5	2.246729	24.197948	0.357696
$NaYF_4$	Y:PST=1:1	2.059803	6.998306	0.035480
	Y:PST=1:4	2.043385	64.590473	0.463362
CaF_2		35.884980	28.125586	0.291264
$BaLuF_5$		2.245110	17.336568	0.298280
$BaYF_5$		2.227641	34.099129	0.284696
$BaGdF_5$		34.566302	27.800114	0.268510

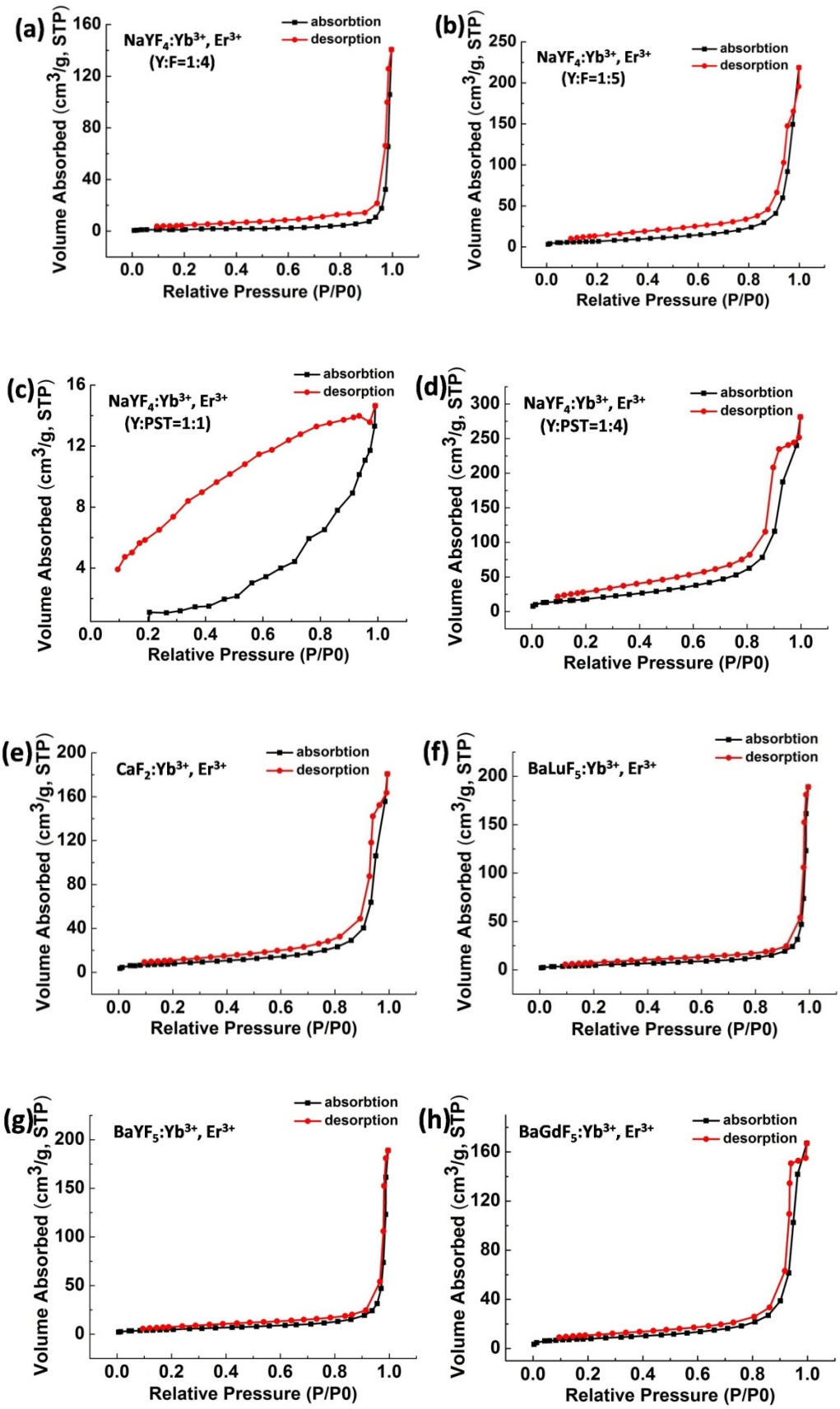
(a)
NaYF4:Yb3+, Er3+
(Y:F=1:4)
absorbtion
desorption
Volume Absorbed (cm3/g, STP)
Relative Pressure (P/P0)
(b)
NaYF4:Yb3+, Er3+
(Y:F=1:5)
absorbtion
desorption
Volume Absorbed (cm3/g, STP)
Relative Pressure (P/P0)
(c)
NaYF4:Yb3+, Er3+
(Y:PST=1:1)
absorbtion
desorption
Volume Absorbed (cm3/g, STP)
Relative Pressure (P/P0)
(d)
NaYF4:Yb3+, Er3+
(Y:PST=1:4)
absorbtion
desorption
Volume Absorbed (cm3/g, STP)
Relative Pressure (P/P0)
(e)
CaF2:Yb3+, Er3+
absorbtion
desorption
Volume Absorbed (cm3/g, STP)
Relative Pressure (P/P0)
(f)
BaLuF5:Yb3+, Er3+
absorbtion
desorption
Volume Absorbed (cm3/g, STP)
Relative Pressure (P/P0)
(g)
BaYF5:Yb3+, Er3+
absorbtion
desorption
Volume Absorbed (cm3/g, STP)
Relative Pressure (P/P0)
(h)
BaGdF5:Yb3+, Er3+
absorbtion
desorption
Volume Absorbed (cm3/g, STP)
Relative Pressure (P/P0)

Figure S1 N_2 adsorption–desorption isotherms for porous UNs, $NaYF_4:Yb^{3+},Er^{3+}$ (Y:F=1:4) (a), $NaYF_4:Yb^{3+},Er^{3+}$ (Y:F=1:5) (b), $NaYF_4:Yb^{3+},Er^{3+}$ (Y:PST=1:1) (c), $NaYF_4:Yb^{3+},Er^{3+}$ (Y:PST=1:4) (d), $CaF_2:Yb^{3+},Er^{3+}$ (e), $BaLuF_5:Yb^{3+},Er^{3+}$ (f), $BaYF_5:Yb^{3+},Er^{3+}$ (g) and $BaGaF_5:Yb^{3+},Er^{3+}$ (h).

Using only water as reaction medium, pH value is an important parameter for morphologies of final products in hydrothermal system. As above experiments (pH=4) show, the products are uniform and monodisperse nanoparticles with the adjustable size. However at the neutral pH=7 and alkaline pH=10 conditions, products morphology varies from nanoparticles to columnar structure in Fig. S2 band Fig. S2d. In the meanwhile, it is noteworthy that morphology of precursors may also be affected very much from dispersive tiny nanoparticles to assemble nanospheres with pH value from 7 to 10, as shown inFig.S2aandFig.S2c. This is probably that variation of pH value will influence complexing effect of PST at the beginning of preparation stage. In strong alkaline environment, the complexation of PST is gradually weakened, resulting in the tiny nanoparticles self-assembling to be bigger loose nanospheres. As we know, PST is prepared from the further processing of tartarisc acid, which is natural fruit acid extracted from residues of grapes. So PST molecules may have better complexing effect at the acidic condition owing to the source of tartaric acid. Our previous experiments also demonstrated that the changes of precursors may influence the final products in hydrothermal reaction. Therefore we can control the products from nanoparticles to rods through simply adjusting pH value of

hydrothermal system. XRD patterns (Fig. S2e) and photoluminescence spectrum (Fig. S2f) can demonstrate the hexagonal products and high upconversion luminous intensity excited by 980nm laser.

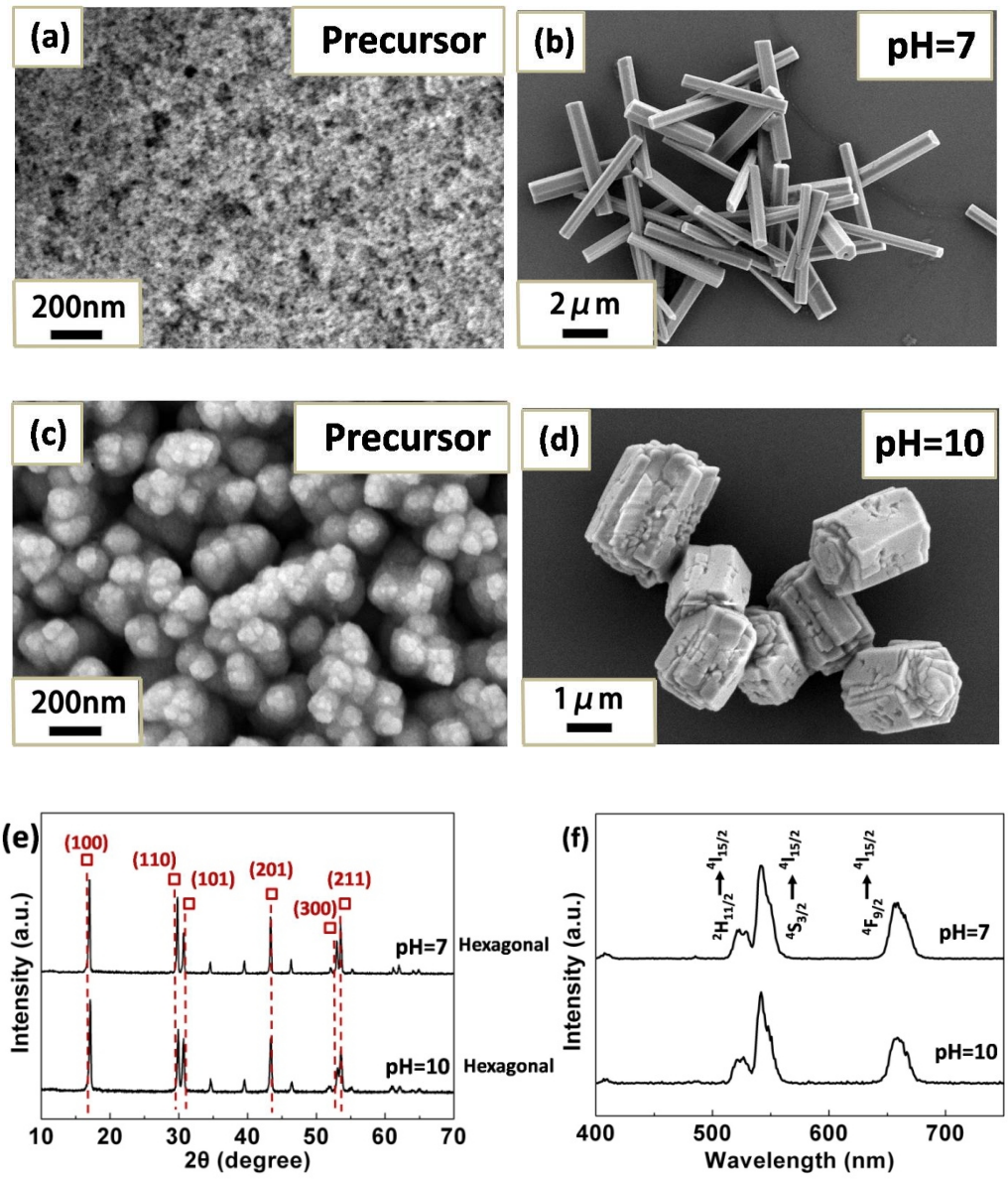

Figure S2 the changes of morphology for $NaYF_4$:Yb^{3+}, Er^{3+} precursors and products at pH =7 and 10, SEM (a) ~ (d). Phase transition (e) and photoluminescence (f) of products at pH=7 and 10, the synthesized products are pure hexagonal phase. (X-ray Diffraction peaks of hexagonal phase are marked with red square boxes).

In order to reveal the effect of fluorine ions on the morphology and phase of UNs, we made a series of experiments at different ratios of F to Y. The results showed the influence process can be divided into two stages: **'precursor stage'** and **'resulting product stage after hydrothermal processing**'. Fig.S3a-c showed the increase of fluorine ions has no obvious influence to the morphology and phase of precursors. In the first stage, when the content of fluorine ions exceed the stoichiometric ratio of $NaYF_4$ (F:Y＞4), these excess fluorine ions may only affiliate on the surface of loose precursors tiny nanoparticles as 'backup equipment' in later hydrothermal system. 'The second stage': after hydrothermal processing, we found that the morphology and phase of UNs varied greatly along with the increased ratio of fluorine to yttrium (Fig. S3d-h). When the proportion of F: Y=4~6, excess fluorine ions have no impact on the morphology, but there some influence on the phase transformation from cubic phase to hexagonal phase, as shown in Fig.S3i. The photoluminescence spectrum (Fig.S3j) was match well with XRD results. With the proportion of (F: Y) increased to 8~12, the morphology changed dramatically from nanoparticles (40-50nm) to micro-prisms, and the phase of products still stay pure hexagonal structure. The peaks intensity of photoluminescence spectrum vary with different proportions of (F: Y), which also

confirm the phase transition from cubic to hexagonal structure. We use FTIR spectra to evaluate the functional groups of porous nanocrystals between 500 and 4000 cm^{-1} (Fig.S3k). The broad absorption band at around 3425 cm^{-1} can be attributed to O-H stretch and the tiny peaks at 2924 and 2850 cm^{-1} indicate the C-H stretching vibrations from the aliphatic chain of PST. The strong peaks at 1609 cm^{-1} can be assigned to the C=O stretching vibrations from carboxylic groups. This means that the PST molecules and its decomposition products provide abundant carboxyl and hydroxyl groups which can be further used in biological coupling and modification.

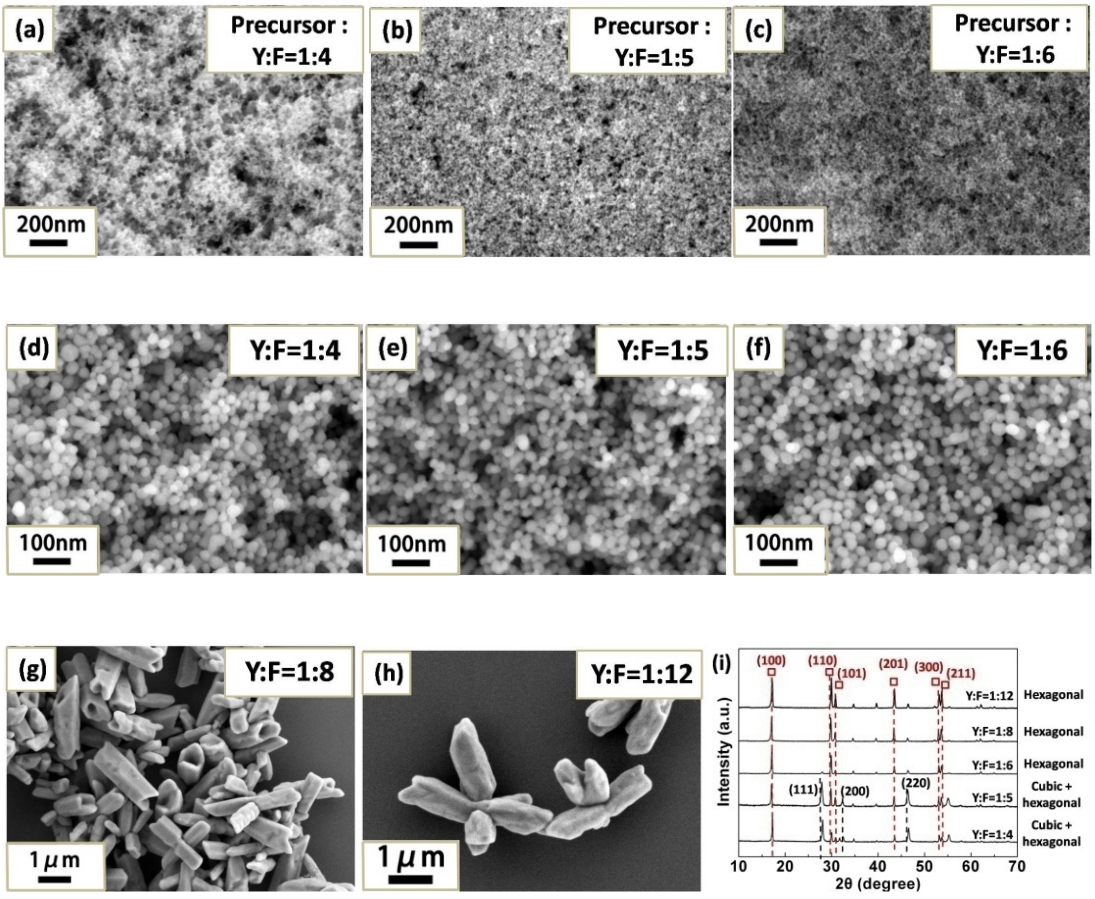

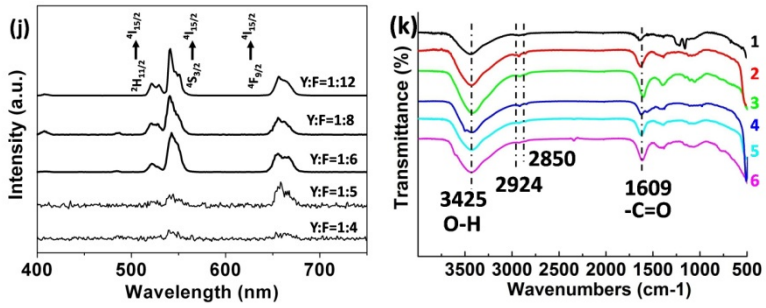

Figure S3 SEM images of precursors at different proportions of F to Y (4, 5 and 6) (a-c), SEM images of resulting products at different proportions of F to Y (4, 5, 6, 8, 12, PST: Y =1, 230 ^{o}C) (d-h). XRD pattern (i) and photoluminescence spectrum (j) of $NaYF_4$:20%Yb^{3+}, 2%Er^{3+} nanocrystals along with the different proportions of Y to Y. FTIR spectrums (k) of precursors and resulting products at the different ratio of F to Y (4, 5 and 6). Note that XRD peaks of hexagonal phase are marked with red square boxes.

Supporting Information Part II:

We make a series of experiments through changing the temperature and F/Y proportions, as shown in Fig. S4. With the increase of hydrothermal temperature, some nanoparticles fuse with each other to some bigger ones or 'attached growth' on the surface of columnar structure, and this process can reduce nanoparticles surface energy efficiently. When increase the proportion (F/Y) from 4 to 6, we can observe distinct morphology transition from nanoparticles to columnar structure. This phenomenon can be explained by our novel mechanism of fluorine ions orientation-absorption which acts as the function of 'assisted rotation', 'morphology shaping role'

and ‘corrosion’. Under the condition of (F/Y=5, 240-260°C), solid columnar structure is common and stable. Under the condition of (F/Y=6, 250-260°C), hollow columnar structure is more stable, which is similar to the ‘pipeline’ that can transport ‘nutrients’ rapidly and balance concentration gradient. This kind of structure is caused by intense ion corrosion effect in hydrothermal system, and the requirement is ‘high energy zone’ such as ‘high temperature’, ‘massive free aggressive ions’ and ‘high ionic activity’.

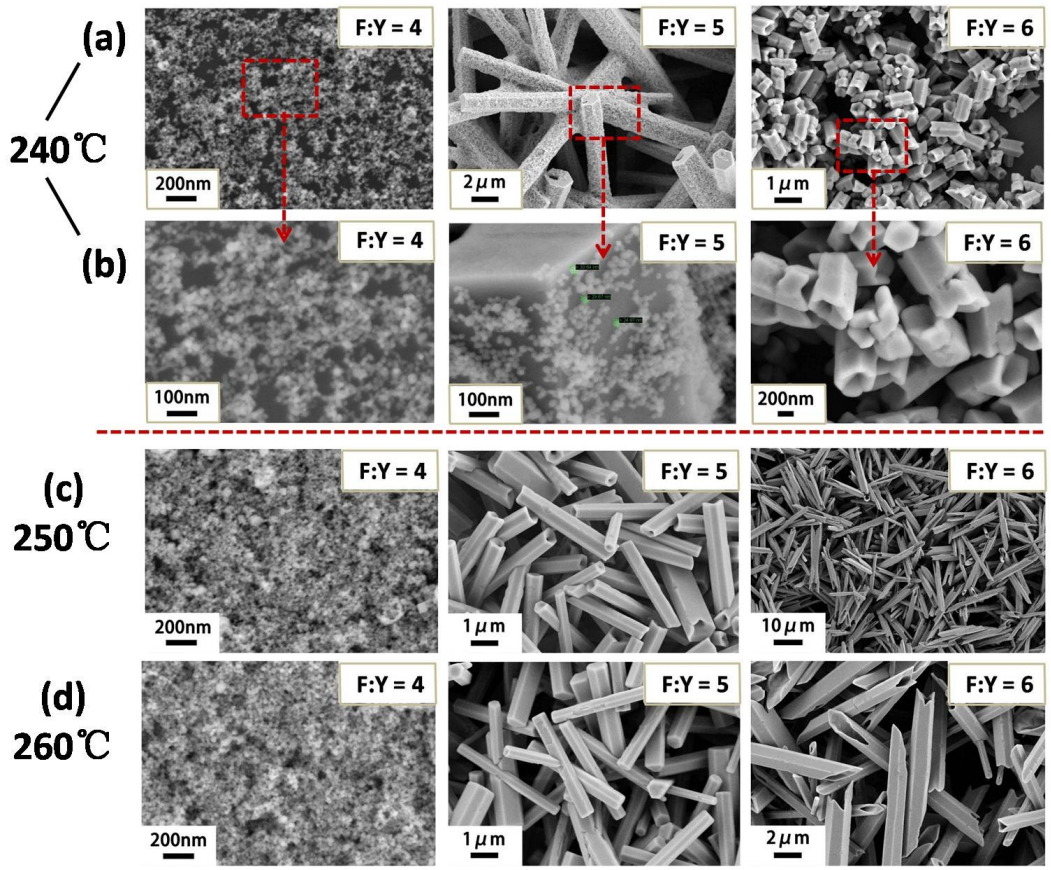

Figure S4 SEM images of the samples at different proportions of F/Y and temperature conditions (a-d).Hydrothermal time was 12 h, only PST was added.

There is no obvious influence for the morphology of $NaYF_4$ nanoparticles through changing hydrothermal reaction time from 12 to 48h as Fig.S5a-c display, but it is noteworthy that phase transition is an evident unusual process along with the extension of hydrothermal time, and variation of photoluminescence intensity can also match with XRD results (Fig.S5d-e). Owing to high temperature and high pressure in reaction kettle, the whole hydrothermal system is in dynamic equilibrium, and there will produce massive waves and fluctuations of energy at any moment. At initial stage of hydrothermal reaction, $NaYF_4$ precursor of cubic phase can gradually jump the energy barrier to form hexagonal phase nanoparticles by means of the outer enormous energy. For $NaYF_4$, when hydrothermal time reaches 12h, almost all of the cubic nucleus will transform to hexagonal phase nanoparticles. While with hydrothermal time further prolonging, massive energy waves may prompt the hexagonal unit cells in $NaYF_4$ nanoparticles to across the energy barriers reversely until most of hexagonal tiny nanocrystals changing into bigger cubic phase. The process of 'reversed jump' is also reasonable and accords with the trend of system energy change, because relatively bigger size can reduce surface energy through fusion and growth as schematic diagram displays in Fig.S5f. From the perspective, we can take full use of this law to prepare pure cubic or hexagonal phase with various sizes and morphologies via changing the hydrothermal reaction time.

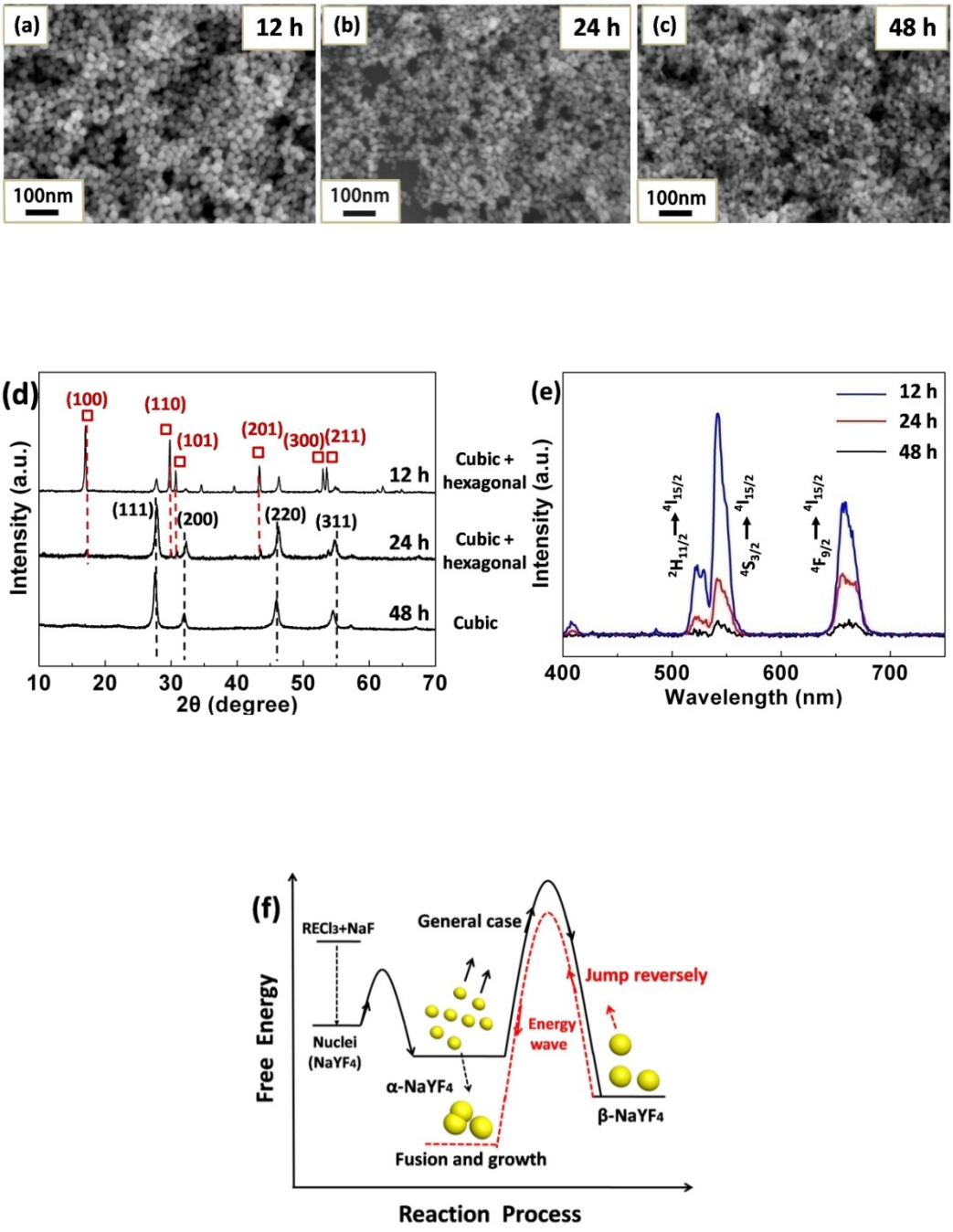

Figure S5 the change of $NaYF_4$ along with different hydrothermal time, (a-c), phase transition (d) and photoluminescence spectrum (e) of $NaYF_4$ from hexagonal phase to cubic phase with hydrothermal time function (12-48h), and the schematic curve (f) for

the specific phase transition. (X-ray diffraction peaks of hexagonal phase are marked with red square boxes).

Supporting Information Part III:

Based on this kind of universal 'Blasting' method, we are also for the first time to synthesize superficially porous CaF_2 nanoparticles (Fig.S6), $BaYF_5$ and $BaGdF_5$ nanoparticles, and $BaLuF_5$nanosheets with good water solubility, which can serve as novel host materials of upconversion nanomaterials in hydrothermal system. It is noteworthy that $BaYF_5$, $BaGdF_5$ and $BaLuF_5$ can also be used as excellent multi-modes imaging contrast agent, such as CT, MRI. Through lanthanide doping into the host materials, CaF_2 as typical fluorite structure also has the upconversion luminescence which can efficiently weaken background fluorescence and enhance signal to noise ratio in *vivo*. Besides, CaF_2 host materials are also excellent biological probes which have good biocompatibility and biotoxicity. Owing to the strong complexation of PST to calcium ions, we prepare water soluble CaF_2:Yb^{3+}, Er^{3+}nanoparticles with perfect crystallinity.

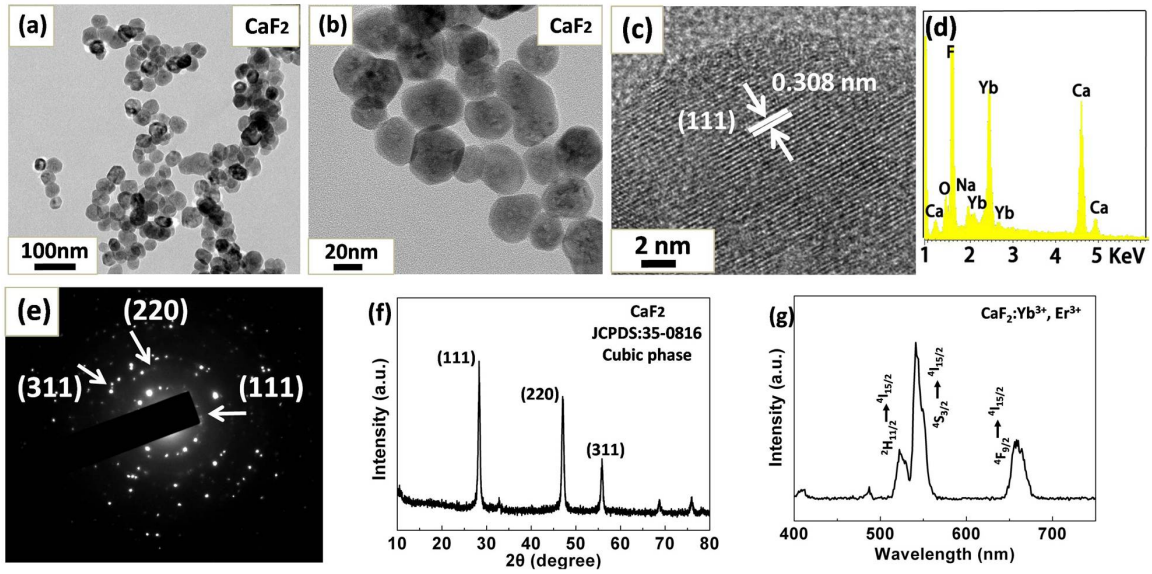

Figure S6 CaF_2:Yb^{3+}, Er^{3+}upconversion nanoparticles (30-40 nm) of TEM (a), local magnification (b), HRTEM (c), EDS (d) and SAED (e). X-ray diffraction pattern (f) and photoluminescence (g) is corresponding to cubic phase of CaF_2.

The whole reaction process of CaF_2can be divided into three stages: (I) 'Assemble stage', (II) 'Inhouse' fusion and 'Swimming' fusion, and (III) 'Crystallize stage'. At the first stage in 1h, tiny precursors nanoparticles will assemble together to form slightly bigger loose amorphous nanocrystals as suggested in Fig. S7a andFig.S7d-e.Then these assembled tiny nanoparticles inside the bigger loose amorphous nanocrystals will fuse to be denser nanospheres with a good crystallinity. It is interesting that some free tiny CaF_2 'nanoclusters' will also 'swim' closely and then adhere to the surface of these fused nanospheres to reduce the whole surface energy, as shown in Fig. S7f-h. In the last stage in 6h, these rare earth ions will sufficiently

dope into the host materials to form homogenous solid solution, and then these nanoparticles have more perfect crystallinity and well-defined shape during the hydrothermal processing. With different hydrothermal time, these rare earth ions (Yb^{3+} and Er^{3+}) can effectively dope into the crystal structure of CaF_2 host materials (Fig. S7i).

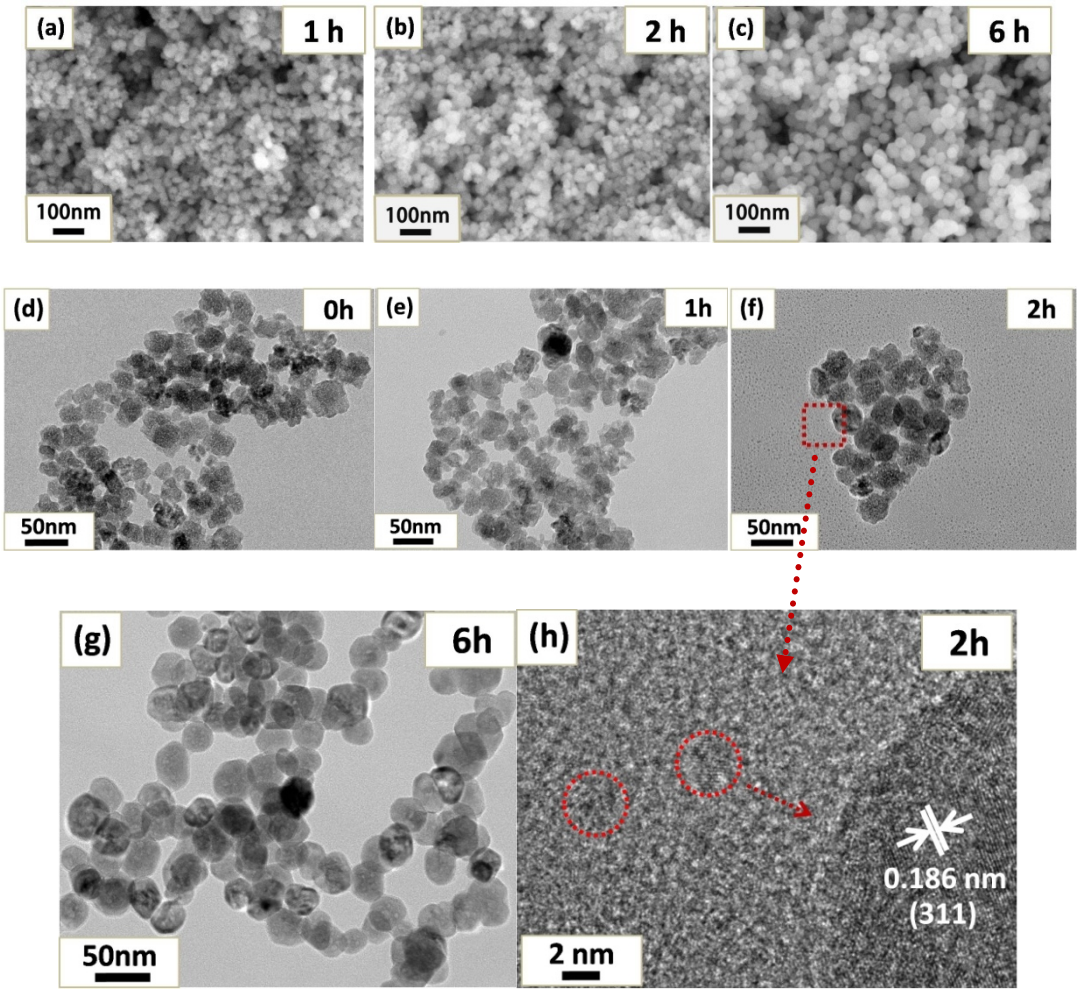

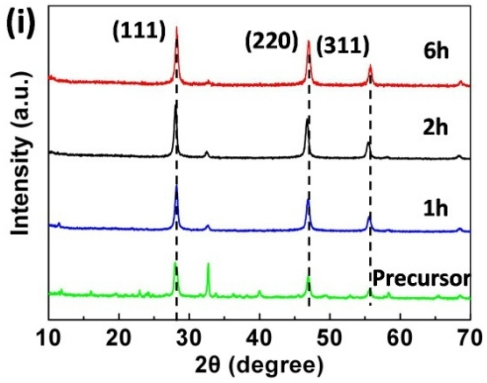

Figure S7 SEM images of CaF_2:Yb^{3+}, Er^{3+}upconversion nanocrystals along with different hydrothermal time (a-c), TEM images (d-g), HRTEM image (h) and XRD patterns (i).

Supporting Information Part IV:

Based on our universal 'Blasting' method, we also have synthesized water-soluble $BaYF_5$, $BaGdF_5$ nanoparticles and $BaLuF_5$nanosheets (thickness:8-10nm), as shown inFig.S8, which can serve as novel host materials of upconversion nanomaterials in hydrothermal system with excellent multi-modes imaging function, such as CT, MRI contrast agents. It is interesting that the morphology of $BaLuF_5$ is thin nanosheet shape not nanoparticles just like the $BaGdF_5$ and $BaYF_5$. This phenomenon can be investigated from the aspect of cubic structure and dipole polarizability. The cubic phase is one type of high-symmetry structure, resulting in less electron cloud

distortion of cations to accommodate the structural change than other structures, such as tetragonal or hexagonal unit cells. Owing to reduced dipole polarizability, heavy lanthanides with small ionic radius may exhibit a less tendency to electron cloud distortion. Compared with Gd^{3+} (r= 0.1193 nm) and Y^{3+}(r= 0.1159 nm), Lu^{3+} (r= 0.0848 nm) ions have smaller ionic radius. Based on above analysis, $BaLuF_5$ may need less energy to form cubic phase nanoparticles, so that the excess energy of outside hydrothermal system will accelerate $BaLuF_5$ nanoparticles to be thin nanosheets as a result of fusion. It is noteworthy to mention that the $BaLuF_5$nanosheets have stronger luminescent intensity under the same condition comparing with $BaGdF_5$ and $BaGdF_5$ nanoparticles. Our preliminary explanation is that structure of nanosheets may stronger activity which may prompt the increase of luminescence intensity.

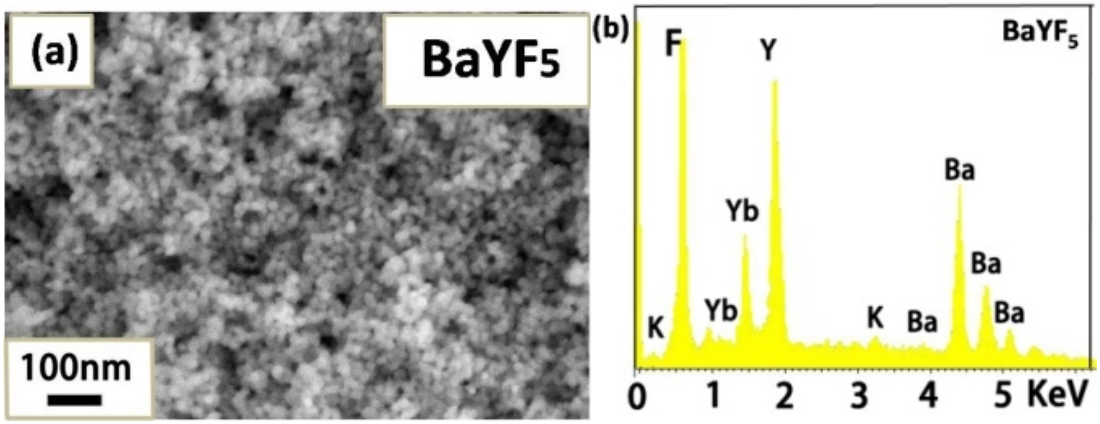

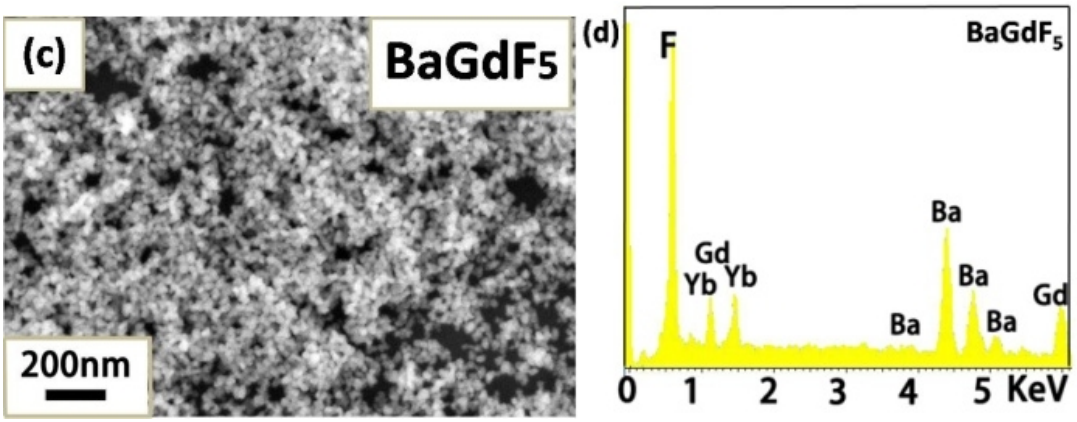
(c)
BaGdF5
200nm
(d)
BaGdF5
F
Gd
Yb
Yb
Ba
Ba
Ba
Ba
Gd
0 1 2 3 4 5 KeV

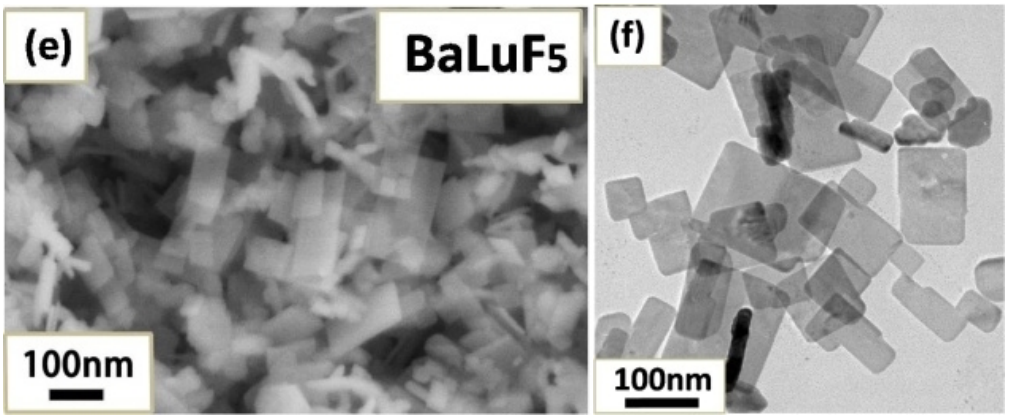
(e)
BaLuF5
100nm
(f)
100nm

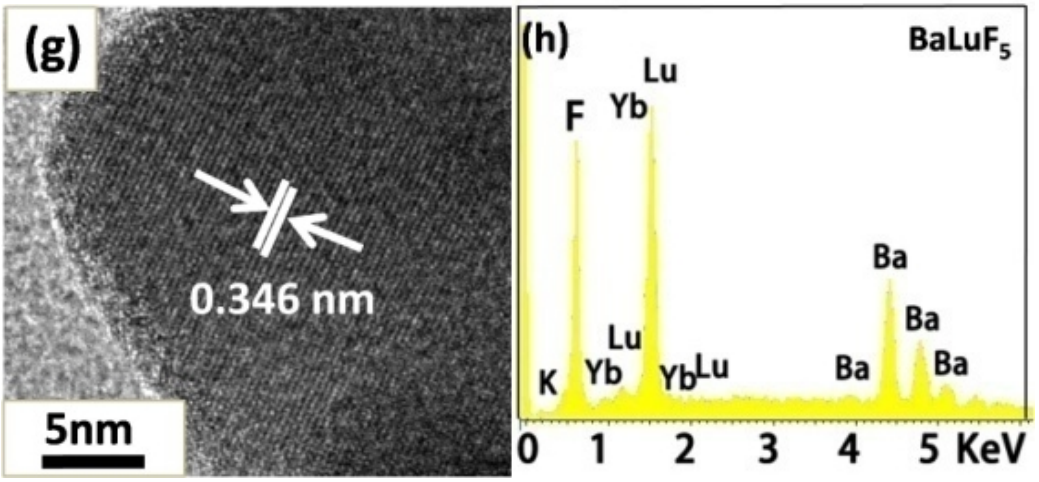
(g)
0.346 nm
5nm
(h)
BaLuF5
F
Yb
Lu
K
Yb
Lu
Yb
Lu
Ba
Ba
Ba
Ba
0 1 2 3 4 5 KeV

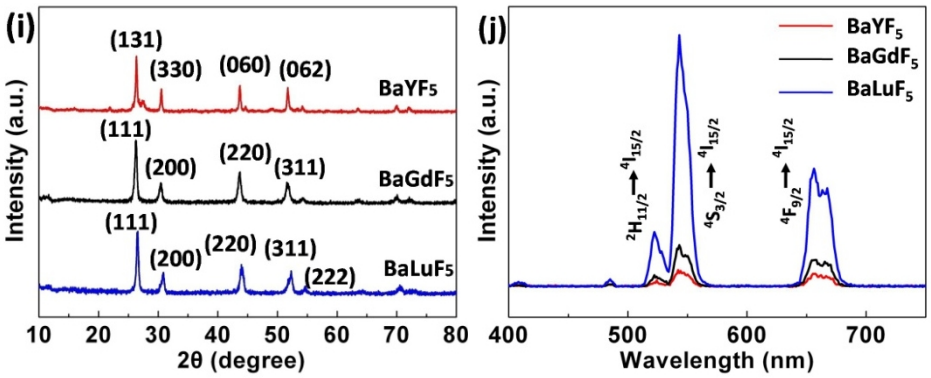

Figure S8 SEM of superficial porous $BaYF_5$:Yb^{3+}, Er^{3+} (a), $BaGdF_5$:Yb^{3+}, Er^{3+} (c) nanoparticles about 25-30nm. EDS of (b) and (d) for $BaYF_5$ and $BaGdF_5$, and the elements include Barium, Yttrium, Gadolinium, Ytterbium, Fluorine and Potassium which comes from PST molecules. SEM (e), TEM (f), HRTEM (g), EDS (h) of $BaLuF_5$:Yb^{3+}, Er^{3+} nanosheets. XRD patterns (i) for $BaYF_5$ nanoparticles (tetragonal phase, JCPDS: 46-0039), $BaGdF_5$ nanoparticles (cubic phase, JCPDS: 24-0098) and $BaLuF_5$nanosheets (cubic phase, ICSD PDF card no. 01-072-3546). Photoluminescence patterns (j) of $BaYF_5$, $BaGdF_5$ and $BaLuF_5$ upconversion nanoparticles excited by 980nm laser.

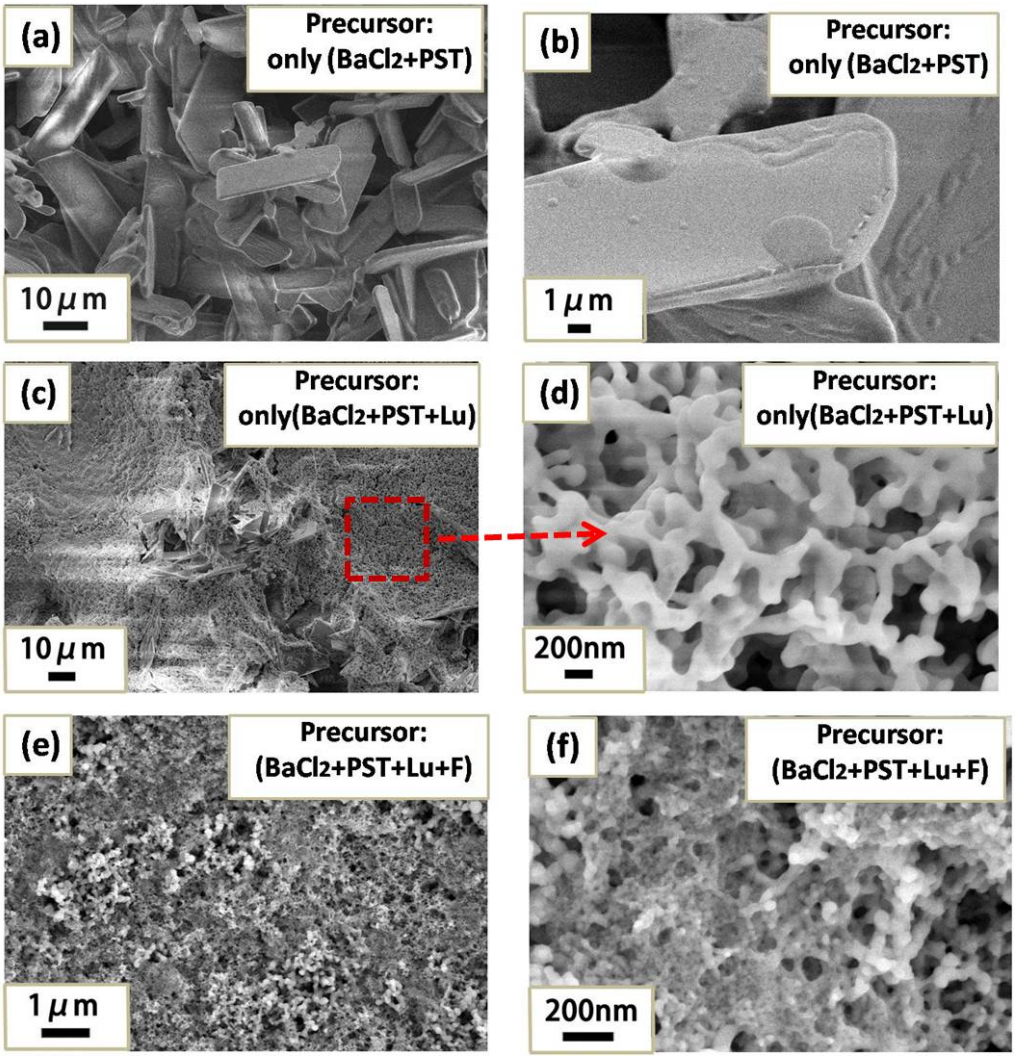

Figure S9 SEM images for $BaLuF_5$:Yb^{3+}, Er^{3+} precursors (a-f).

Here, we can directly observe and investigate the variation at three different synthesized stages of precursors, as shown in Fig. S9 a-f. In fact, barium chloride ($BaCl_2$) exists in the form of big crystal clear wafers, and then it will become small 'skateboard' shape when adequately mixing with PST solution. When lutecium chloride ($LuCl_3$) solution is added into above mixed solution, Lu^{3+}ions have strong

complexation with PST molecules to form 'network structure' as the local magnification (Fig.S9d). After that, we dropwise add the sodium fluoride (NaF) solution into aforementioned system, we obtain tiny precursor nanoparticles, and then these amorphous precursors will grow up and crystallize to be $BaLuF_5$ nanoparticles products. With extension of hydrothermal time, these nanoparticles will fuse together to be final morphology of nanosheets.

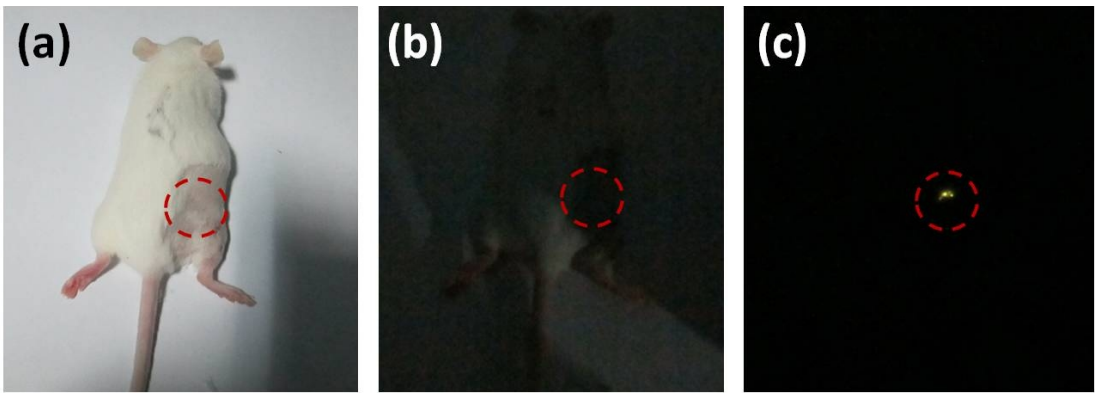

Figure S10 *In vivo* optical imaging through subcutaneous injection with $NaYF_4$:Yb^{3+}, Er^{3+} upconversion nanoparticles.